Comment

Hydrogenated amorphous boron nitride: A first principles study

Tevhide Ayça Üçhöyük, Murat Durandurdu*

Department of Materials Science & Nanotechnology Engineering, Material Science & Mechanical Engineering Program, Abdullah Gül University, Kayseri 38080, Turkey

ABSTRACT

The influence of hydrogenation on the atomic structure and electronic properties of amorphous boron nitride (*a*-BN) is investigated by using an ab-initio molecular dynamics technique. The structural evaluation of *a*-BN and the hydrogenated (*a*-BN:H) models with four different hydrogen concentrations reveals that although their short-range order is mainly similar to each other, hydrogenation yields some noticeable amendments on the local structure of *a*-BN. Hydrogenation suppresses the formation of twofold coordinated chain-like structures and tetragonal-like rings and leads to more sp^2 and even sp^3 hybridizations. It is also observed that the formation of N−H bonding is more favorable than that of the B−H bonding in the *a*-BN:H configurations. Furthermore hydrogenation is found to have an insignificant impact on the electronic structure of *a*-BN.

1. Introduction

Boron Nitride (BN), a III-V compound, is a synthetic material having crystal structures similar to carbon. It is a wide band gap semiconductor. Due to its unique physical and chemical features, it has been attracted a great deal of scientific and advanced technological interests. It is one of promising candidates as a superhard material after diamond.

BN forms four different crystal structures: hexagonal (h-BN), rhombohedral (r-BN), cubic (c-BN) and wurtzite (w-BN) [1]. The ground state structure of BN is the h-BN phase being a two-dimensional layered material with a weak Van der Waals force [2]. h-BN has various superior features [3]. The rhombohedral BN (r-BN) also forms in a two-dimensional structure [4], similar to h-BN. Amongst the other phases, r-BN is the least understood one [5]. Cubic BN (c-BN) can be manufactured from h-BN and r-BN at high temperature and pressure conditions [6]. Due to its extreme hardness, it can be used as a protective coating of heavy-duty tools [7]. The high pressure and temperature treatments can possess a phase transformation from h-BN to a wurtzite structure (w-BN) as well [8], which can be classified as a superhard material.

Amorphous BN (*a*-BN) can be synthesized using various experimental techniques such as high frequency chemical vapour deposition and ball milling [9–11] but relative to the crystalline forms, it has been little explored and hence less understood [12–17]. Amorphous materials have coordination defects and strained topologies, which significantly influence their electrical and physical properties. Their main coordination defect is undercoordinated atoms i.e. dangling bonds. Hydrogenation somehow not only passivates the dangling bonds but also breaks strained and weak bonds in amorphous materials and yields more ordered configurations [18]. Such hydrogenation induced structural changes improve significantly their physical and electrical properties. Consequently hydrogenated *a*-BN (*a*-BN:H) has been studied experimentally as well [19,20]. Although there are few theoretical studies on *a*-BN [21,22] to shed some light on its atomic structure and electronic properties, to our knowledge, there has been no attempt to investigate theoretically *a*-BN:H. Thus currently the impact of hydrogenation on the atomic structure and electric properties of *a*-BN is not well known. And hence in this work, we generate *a*-BN:H with four different hydrogen contents based on an ab initio technique and compare them structurally and electronically with pure *a*-BN to fill the gap in the literature. We find that hydrogenation induces drastic structural changes in the network compared to pure *a*-BN. Yet in spite of the changes, hydrogenation is found to have a small influence on its electronic properties.

2. Methodology

The SIESTA package [23] based on the density functional theory (DFT) was used to perform molecular dynamics (MD) simulations. The atomic orbital basis set was selected as a double-zeta plus polarized (DZP) orbital for the valance electrons. The pseudopotentials were produced by the Troullier and Martins approach [24]. The Becke gradient exchange functional [25] and Lee, Yang, and Parr correlation functional [26] were applied to estimate the exchange correlation energy. The MD simulations were performed within the NPT (isothermal-isobaric) ensemble in which temperature and pressure were controlled

by the velocity scaling and the Parrinelo-Rahman techniques [27], respectively. The time step of each MD simulation was set to 1.0 fs. We chose a 216-atom liquid BN model (108 B atoms and 108 N atoms) at 3300 K as an initial structure. We removed arbitrarily 5 B and 5 N atoms from the melt, replaced 14, 22, 30 and 46H atoms and created 220, 228, 236,252-atoms models that were labeled as model1, model2, model3 and model4, respectively. The hydrogen concentration is about 6.4, 9.6, 12.7 and 18.2% for the model1, model2, model3 and model4, correspondingly. Experiment [20] suggested the existence of 5–10% hydrogen in a-BN:H film. So the model1 and model2 consist of a H concentration in the experimental range. On the other hand, model2 and model3 have a higher H concentration than the experimental proposition and hence they can be considered as a hypostatical structure but they actually allow us to understand the impacts of excessive hydrogenation on the local structure of the amorphous network. All initial configurations were subjected to 3300 K for 50.0 ps and then the melts were gradually cooled to 300 K within 150.0 ps. Finally these structures were relaxed according to the force criteria of 0.01 eV/Å. The relaxed structures' density is 2.0430 g/cm^3 for pure *a*-BN, 1.8033 g/cm^3 for model1, 1.9063 g/cm^3 for model2, 1.7055 g/cm^3 for model3, and 1.8345 g/cm^3 for model4. They are indeed reasonably comparable with the experimental value of 1.9 ± 0.1 g/cm^3 [19].

3. Results

In order to distinguish the short-range order of the *a*-BN:H configurations from that of pure (unhydrogenated) *a*-BN, we first consider the partial pair distribution functions (PPDFs) and plot them in Fig.1 (more visible PPDFs are provided in the supplementary document). The first peak position of all correlations of the *a*-BN:H models along with that of h-BN and pure *a*-BN model is summarized in Table 1. One can see that the distances estimated are quite close to each other, suggesting that the *a*-BN:H structures are locally similar to pure *a*-BN [21] and h-BN [28]. The B−H and N−H bond lengths are located at around 1.17 Å and

Table 1
The first peak position of correlations.

	B-B (Å)	B-N (Å)	N-N (Å)	B-H (Å)	N-H (Å)	H-H (Å)
h-BN	2.50	1.57	2.50			
pure *a*-BN	2.51	1.46	2.54			
Model 1	2.50	1.43	2.51	1.17	0.98	1.95
Model 2	2.51	1.43	2.52	1.16	0.98	1.74
Model 3	2.49	1.43	2.50	1.17	0.97	1.65
Model 4	2.51	1.44	2.52	1.17	0.98	1.68

0.98 Å, respectively for the all *a*-BN:H networks. These values are comparable with 1.17 Å for B−H bond length and 1.03 Å for N−H bond distance reported in a neutron diffraction study of BH$_3$NH$_3$ [29]. The position of the H−H correlation at near 1.65–1.95 Å indicates that the models are free from H−H bonds because H−H bond length is 0.74 Å. From the PPDFs, one can see that these models do not form any N−N bond as well but have a small amount of B−B homopolar bonds as denoted by a feeble peak at 1.70–1.74 Å in the B−B correlation, similar to what has been observed for pure *a*-BN [21]. The fraction of B−B bonds in *a*-BN:H is however slightly higher than that of *a*-BN. The PPDF analyses suggest that the correlation distances are not affected by hydrogenation.

The coordination number (CN) is an essential feature to describe the short-range order of disordered systems. Using the first minimum of the PPDFs (~1.86 Å for B−B, ~2.02 Å for B−N, ~1.57 Å for B−H and 1.49 Å for N−H correlations), we estimate the total and partial CNs. Fig. 2 illustrates the coordination distributions of the *a*-BN:H models and the *a*-BN network. For the pure *a*-BN configuration, the frequency of twofold, threefold-, and fourfold-coordinated atoms is 6%, 91%, and 3%, correspondingly. The subsequent average CN is 2.97. By hydrogenation, one can perceive a decrease in the number of dangling bonds (twofold chain-like configurations) and almost no twofold coordinated atoms for the model3 and model4. Hydrogenation leads to more sp^2 and
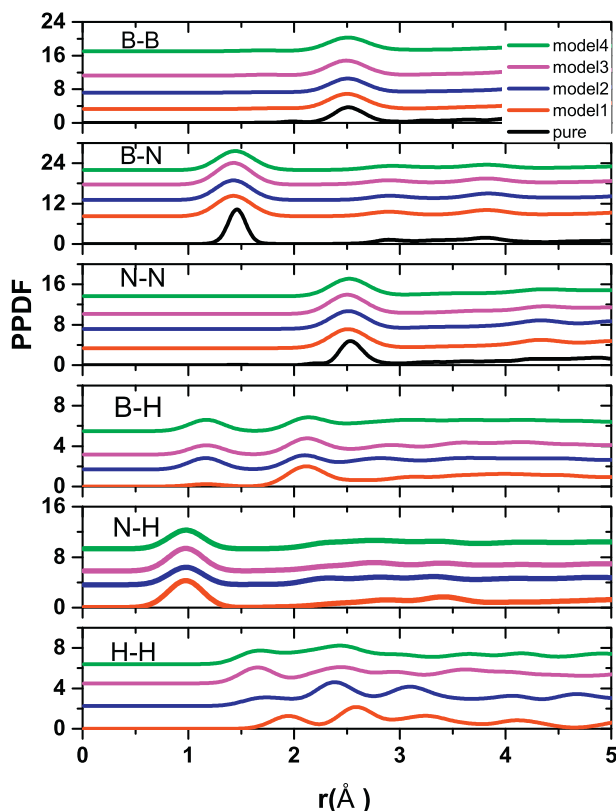

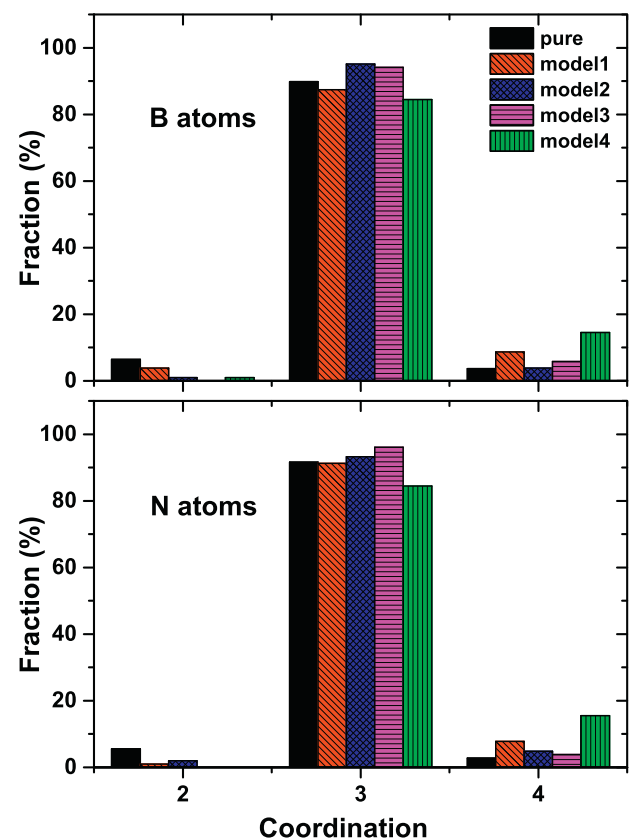**Fig. 1.** PPDFs of the pure *a*-BN and *a*-BN:H models.

Fig. 2. Coordination distribution of the pure *a*-BN and *a*-BN:H models.

even sp³ hybridizations in the first three models, relative to pure *a*-BN. Their mean CN is about 3.03–3.06. The situation for model4 is slightly different: 85% of atoms are threefold coordinated and about 15% of atoms (15% of B atoms and 16% of N atoms) are fourfold coordinated. The average B and N CNs are 3.13 and 3.15, correspondingly. For this model, we find that the at least 50% of sp³ configurations involve at least one H atom while the rest occurs between B and N atoms. The B−N₄, B-N₃H, N−B₄, N-B₃H and N-B₂H₂ configurations are the main sp³ hybridization units in the model. For intermediate hydrogen concentration, similar trend has been reported for hydrogenated amorphous carbon (*a*-C:H) called as hydrogenated diamond-like carbon (DLC) films, in which hydrogenation yields more sp³ C−C bonding [30].

All H atoms are onefold coordinated and a close investigation reveals the fact that there are more N−H bonding than B−H bonding in all *a*-BN:H models; about 65–93% of H atoms form a bond with N atoms. The model1 presents the highest fraction of N−H bonding (93%) while model4 shows the lowest one (65%). Actually we find a correlation between H concentration and the number of N−H bonds (or B−H bonds) formed in the amorphous systems: the frequency of N−H bonds decreases with increasing H concentration.

To further understand the atomic structure of *a*-BN:H in details, we explore the bond angle distribution functions (BADFs). The B−N−B and N−B−N angle distributions are provided in Fig.3. The main peak of all *a*-BN:H models are located at around 116°–119°, indicating that *a*-BN:H has an atomic arrangement related to that of h-BN. Note that the hydrogenated configurations (model1, model2 and model3) produce a sharper peak around 120° than the pure *a*-BN model, suggesting that hydrogenation yields a more ordered local structure in the system. We also note here that while the pure *a*-BN network has a subpeak at about 80° for the B-N-B and 95° for N-B-N because of the presence of the tetragonal rings [20], the *a*-BN:H models do not present such peaks in the BADFs, indicating that hydrogenation suppress the development of
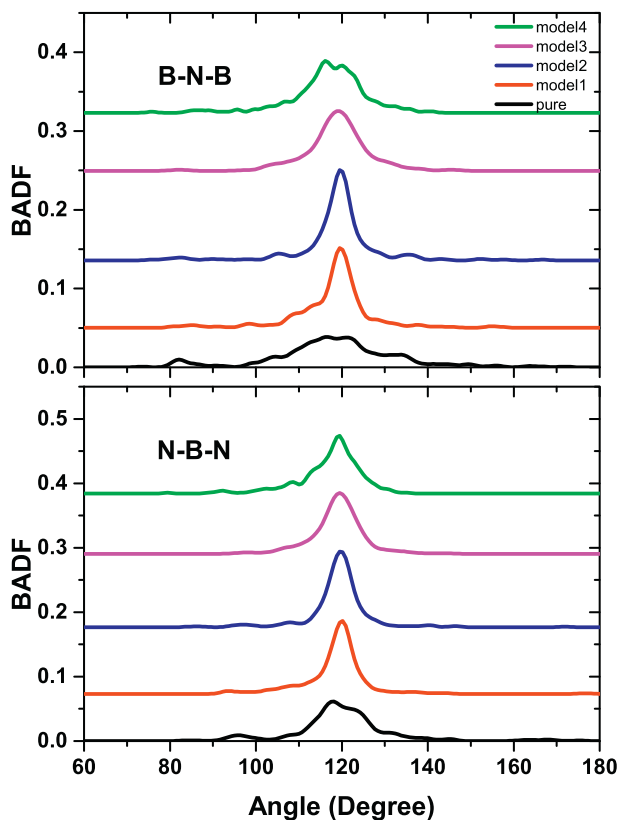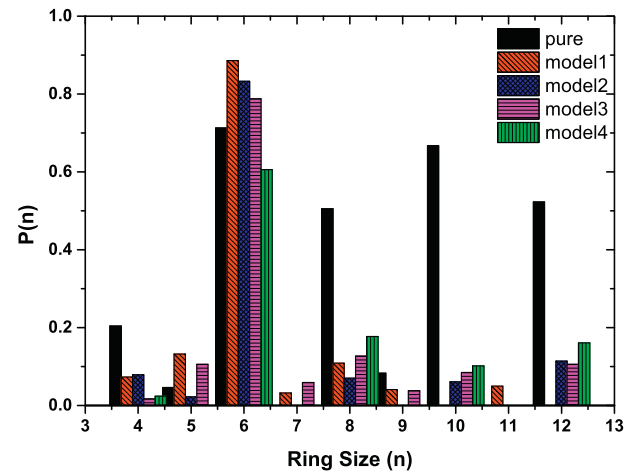

Fig. 4. Ring distribution of the pure *a*-BN and *a*-BN:H models.

tetragonal rings as well. This is further supported by the rings analysis as shown in Fig.4. Four membered rings exist in pure *a*-BN but the fraction of such rings is negligibly small in the *a*-BN:H models.

To understand the effects of hydrogenation on the electronic properties of *a*-BN, we lastly compute the electronic density of states (EDOS) of the models and demonstrate them in Fig.5. We also provide the EDOS of pure *a*-BN and h-BN in the figure for comparison purpose. The band gap energy defined as the difference of HOMO-LUMO states is found to be about 4.5 eV for h-BN and ~2.0 eV for pure *a*-BN. It should be pointed out here that DFT-GGA calculations underestimate band gap widths and hence they are not comparable with experimental values. For the *a*-BN:H models, we do not perceive a drastic modification in the band gaps except that a midgap state is presented in model3. The band gap of the *a*-BN:H configurations is close to that of pure *a*-BN and about 1.8–2.0 eV. A close analysis of the midgap state using the localization of wavefunctions reveals that it is indeed due to a chain-like B−B structure formed in model3 (see Fig. 6). We should note here that such a chain-like structure does not exist in other models although they present a small amount of B−B homopolar bonds.

To shed additional lights on the electronic properties of the *a*-BN and *a*-BNH models, we probe the partial density of states (PDOS) provided in Fig. 7. The eigenstates near −20 eV are mainly due to N-s states. B-s and B-p states have some contributions to these energy levels as well. The valance band has contributions from B-s, B-p and essentially N-p states. The conduction band near Fermi level is controlled by B-p states. Our observations are quite similar to what have been stated for h-BN in a previous simulation [31]. The contribution of H atoms to
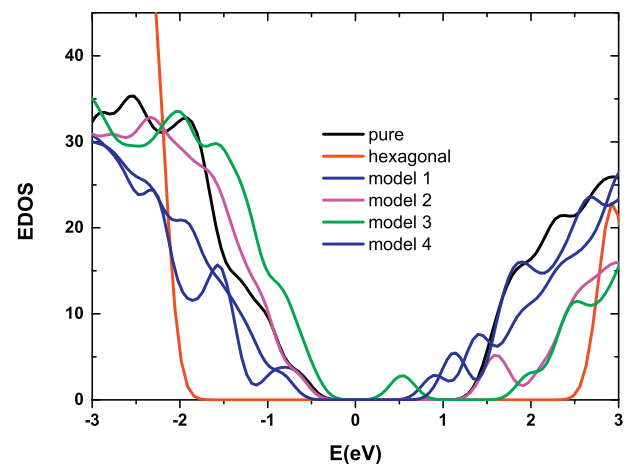

Fig. 3. BADF of the pure *a*-BN and *a*-BN:H models.

Fig. 5. EDOS around the Fermi level for h-BN, *a*-BN and *a*-BN:H models.
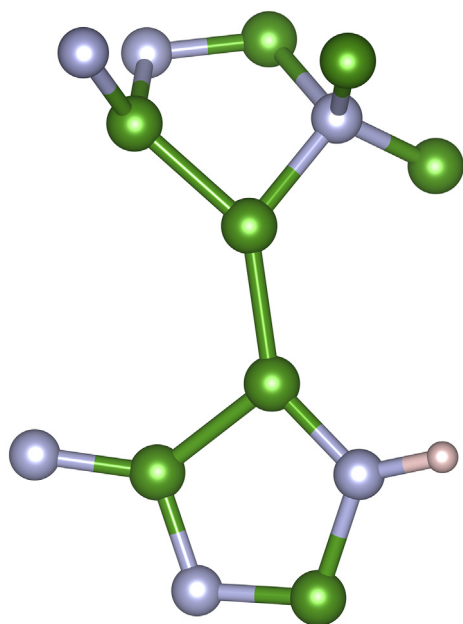
Fig. 6. Chain-like B—B structure produces the midgap state in model3.
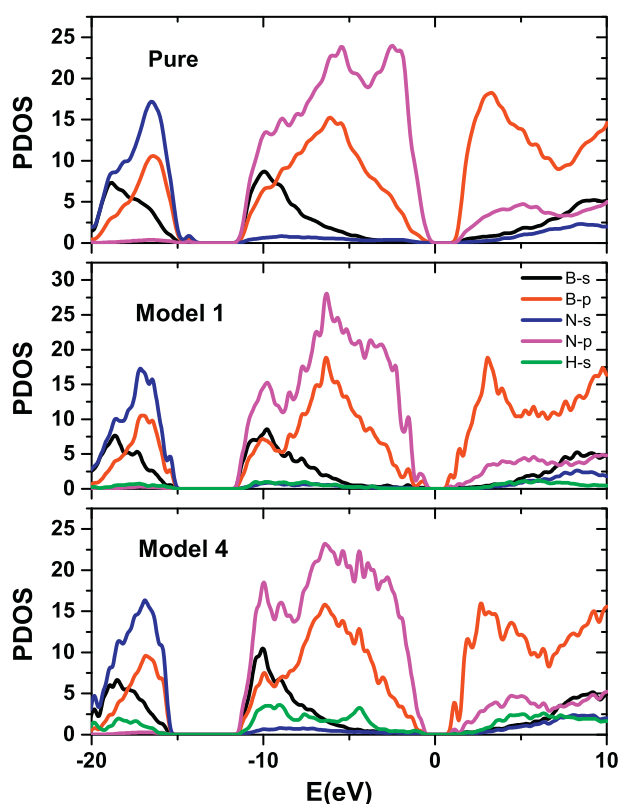

Fig. 7. PDOS of selected models.

the PDOS is significantly small.

4. Discussion

On the basis of the structural analyses, we suggest that the main building unit of both *a*-BN:H and pure *a*-BN is hexagonal rings similar to h-BN. Yet there are some noticeable structural differences between *a*-BN:H and *a*-BN. As expected, hydrogenation passivates twofold-co-ordinated configurations and yields more sp^2 bonding. In addition, it induces a few sp^3 bonding in the models. Yet as for the hydrogenated content of 18.2%, a noticeable increase in the fraction of sp^3 hybridization is observed in the network. Here based on the observation of the sp^2-to-sp^3 transition in BN at high temperature and pressure treatments, we speculate that the physical origin of such a behavior is probably due to the high degree of stress caused by the excessive hydrogen content in the network. However, further investigations are needed to fully clarify this issue. The development of more sp^3 bonding can be interpreted as some improvement to the mechanical properties of the amorphous configurations because the BN crystals having sp^3 hybridization are a superhard material.

We observe that the formation of N—H bonding is more favorable than that of B—H bonding in all models. This behavior might be unsurprising and can be simply explained by bond energy. Based on bond energy [32], N—H bonding (347 ± 13 kj/mol) is energetically more favorable than B—H bonding (289 ± 38 kj/mol).

Since the bonding nature of BN has significant impacts on its physical, chemical, mechanical and electronic properties, perhaps by changing hydrogen content, *a*-BN:H with different features can be engineered.

5. Conclusions

We have generated *a*-BN:H models with four different hydrogen concentrations by means of a first-principles MD approach. The comparison of the *a*-BN:H configurations with *a*-BN reveals that although they are locally parallel to each other, hydrogenation yields some noticeable changes on the local structure of *a*-BN. Due to the H passivation of dangling bonds, the *a*-BN:H models do not form the twofold co-ordinated chain-like structures. Furthermore it suppresses the development of tetragonal-like rings. All these structural modifications lead to more sp^2 and even sp^3 hybridizations. Because of higher sp^3 bonding, *a*-BN:H is anticipated to possess better mechanical properties than pure *a*-BN. Additionally we witness the formation of more N—H bonds than B—H bonds in the hydrogenated models. Considering the electronic properties, hydrogenation is found to have minor impact on the electronic structure of *a*-BN.

Acknowledgements

Appendix A. Supplementary data

Supplementary data to this article can be found online at https://doi.org/10.1016/j.jnoncrysol.2018.08.021.

References

[1] B.T.T. Kelly, Physics of graphite, J. Nucl. Mater. 114 (1) (1983) 1983.
[2] K.K. Kim, et al., Synthesis of monolayer hexagonal boron nitride on Cu foil using chemical vapor deposition, Nano Lett. 12 (1) (2012) 161–166.
[3] G. Cassabois, P. Valvin, B. Gil, Hexagonal boron nitride is an indirect bandgap semiconductor, Nat. Photonics 10 (4) (Apr. 2016) 262–266.
[4] Y. Matsui, Y. Sekikawa, T. Sato, T. Ishii, S. Isakosawa, K. Shii, Formations of rhombohedral boron nitride, as revealed by TEM-electron energy loss spectroscopy, J. Mater. Sci. 16 (4) (1981) 1114–1116.
[5] V.L. Solozhenko, I.A. Petrusha, A.A. Svirid, Thermal phase stability of rhombohedral boron nitride, High Pressure Res. 15 (2) (1996) 95–103.
[6] R.H. Wentorf, Synthesis of the cubic form of boron nitride, J. Chem. Phys. 34 (3) (1961) 809–812.
[7] R. Ahmed, F.-E. Aleem, S. Javad Hashemifar, H. Akbarzadeh, First principles study of structural and electronic properties of different phases of boron nitride, Phys. B 400 (2007) 297–306.
[8] F.P. Bundy, R.H. Wentorf, Direct transformation of hexagonal boron nitride to denser forms, J. Chem. Phys. 38 (5) (1963) 1144–1149.
[9] J.Y. Huang, H. Yasuda, H. Mori, HRTEM and EELS studies on the amorphization of

hexagonal boron nitride induced by ball milling, J. Am. Ceram. Soc. 83 (2) (2000) 403–409.

[10] S.-I. Hirano, T. Yogo, S. Asada, S. Naka, Synthesis of amorphous boron nitride by pressure pyrolysis of borazine, J. Am. Ceram. Soc. 72 (1) (1989) 66–70.

[11] R. Zedlitz, M. Heintze, M.B. Schubert, Properties of amorphous boron nitride thin films, J. Non-Cryst. Solids 198–200 (1996) 403–406.

[12] E.J.M. Hamilton, S.E. Dolan, C.M. Mann, H.O. Colijn, C.A. McDonald, S.G. Shore, Preparation of amorphous boron nitride and its conversion to a turbostratic, tubular form, Science (80-.). 260 (5108) (1993) 659–661.

[13] H. Lorenz, I. Orgzall, In situ observation of the crystallization of amorphous boron nitride at high pressures and temperatures, Scr. Mater. 52 (6) (2005) 537–540.

[14] D.R. Ketchum, A.L. DeGraffenreid, P.M. Niedenzu, S.G. Shore, Synthesis of amorphous boron nitride from the molecular precursor ammonia-monochloroborane, J. Mater. Res. 14 (5) (1999) 1934–1938.

[15] A. Werbowy, J. Szmidt, A. Sokolowska, A. Olszyna, S. Mitura, Fabrication and properties of Mo contacts to amorphous cubic boron nitride (a-cBN) layers, Diam. Relat. Mater. 5 (9) (1996) 1017–1020.

[16] T. Taniguchi, K. Kimoto, M. Tansho, S. Horiuchi, S. Yamaoka, Phase transformation of amorphous boron nitride under high pressure, Chem. Mater. 15 (14) (2003) 2744–2751.

[17] S.K. Singhal, J.K. Park, Synthesis of cubic boron nitride from amorphous boron nitride containing oxide impurity using Mg-Al alloy catalyst solvent, J. Cryst. Growth 260 (1–2) (2004) 217–222.

[18] M. Legesse, M. Nolan, G. Fagas, A first principles analysis of the effect of hydrogen concentration in hydrogenated amorphous silicon on the formation of strained Si-Si bonds and the optical and mobility gaps, J. Appl. Phys. 115 (20) (May 2014) 203711.

[19] S.W. King, M. French, J. Bielefeld, M. Jaehnig, M. Kuhn, B. French, X-ray photoelectron spectroscopy investigation of the Schottky barrier at a-BN:HCu interfaces, Electrochem. Solid-State Lett. 14 (12) (2011).

[20] S.W. King, et al., Valence band offset at the amorphous hydrogenated boron nitride-silicon (100) interface, Appl. Phys. Lett. 101 (4) (2012).

[21] M. Durandurdu, Hexagonal nanosheets in amorphous BN: a first principles study, J. Non-Cryst. Solids 427 (2015) 41–45.

[22] D.G. McCulloch, D.R. McKenzie, C.M. Goringe, Ab initio study of structure in boron nitride, aluminum nitride and mixed aluminum boron nitride amorphous alloys, J. Appl. Phys. 88 (9) (2000) 5028–5032.

[23] J.M. Soler, et al., The SIESTA method for ab initio order-N materials simulation, J. Phys. Condens. Matter 14 (11) (2002) 2745–2779.

[24] J.M.N. Troullier, Efficient pseudopotentials for plane-wave calculations, Phys. Rev. B 43 (3) (1991) 1991–1997.

[25] A.D. Becke, Density-functional exchange-energy approximation with correct asymptotic behavior, Phys. Rev. A 38 (6) (1988) 3098–3100.

[26] C. Lee, W. Yang, R.G. Parr, Development of the Colle-Salvetti correlation-energy formula into a functional of the electron density, Phys. Rev. B 37 (2) (1988) 785–789.

[27] M. Parrinello, A. Rahman, Polymorphic transitions in single crystals: a new molecular dynamics method, J. Appl. Phys. 52 (12) (1981) 7182–7190.

[28] Y. Kumashiro (Ed.), Electric Refractory Materials, Taylor & Francis, New York, 2000.

[29] W.T. Klooster, T.F. Koetzle, P.E.M. Siegbahn, T.B. Richardson, R.H. Crabtree, Study of the N-H··H-B dihydrogen bond including the crystal structure of BH3NH3 by neutron diffraction, J. Am. Chem. Soc. 121 (27) (1999) 6337–6343.

[30] Y.R. Jueyuan, Overview of amorphous carbon films, Ultrathin Carbon-Based Overcoats for Extremely High Density Magnetic Recording, Springer, Singapore, 2017, pp. 29–37.

[31] M. Topsakal, E. Aktürk, S. Ciraci, First-principles study of two- and one-dimensional honeycomb structures of boron nitride, Phys. Rev. B - Condens. Matter Mater. Phys. 79 (11) (2009).

[32] B. de Darwent, *Bond Dissociation Energies in Simple Molecules*, National Bureau of Standards, 1970.